

SCIENTIFIC REPORTS

OPEN

Coexistence of spin ordering on ladders and spin dimer formation in a new-structure-type compound $\text{Sr}_2\text{Co}_3\text{S}_2\text{O}_3$

Kwing To Lai & Martin Valldor

Received: 24 August 2016

Accepted: 30 January 2017

Published: 03 March 2017

We report on the syntheses and characterizations of single crystalline and polycrystalline $\text{Sr}_2\text{Co}_3\text{S}_2\text{O}_3$ with a novel crystal structure type. It contains Co–O 2-leg rectangular ladders and necklace ladders. The two ladders share common legs and construct a *hybrid spin ladder*. A rare meridional heteroleptic octahedral coordination is found for the Co^{2+} ions in the 2-leg ladder. Within the necklace ladders, the Co^{2+} ions are in *trans*-octahedral coordination. An antiferromagnetic order is observed at $T_N \sim 267$ K, while a broad maximum in magnetic susceptibility is found below T_N . This relatively high ordering temperature among Co-based ladder compounds is related to the highly anisotropic *mer*-coordination of the Co^{2+} ions. The *trans*-octahedrally coordinated Co^{2+} ions, on the other hand, corresponds to the possible short-range magnetic correlations through dimers with an effective $S = \frac{3}{2}$. This results in a rare situation that spin ordering and spin dimers coexist down to 2 K.

High-spin Co^{2+} ($3d^7$) has a spin angular momentum $S = \frac{3}{2}$ and an orbital angular momentum $L = 3$ according to Hund's rules. With the cooperation of octahedral crystal field and spin-orbital coupling, the lowest-lying orbital level of Co^{2+} splits into a Kramers doublet, a quartet and a sextet. The Kramers doublet ground state has an effective $S = \frac{1}{2}$ with large Ising-type anisotropy and is separated with the first excited quartet (effective $S = \frac{3}{2}$) by a energy gap of about 10^2 K order of magnitude^{1–4}. Hence, low dimensionality in octahedral Co^{2+} compounds can yield novel properties due to the strong quantum fluctuations for $S = \frac{1}{2}$ systems. For instance, the quasi one-dimensional (1D) $S = \frac{3}{2}$ screw chain antiferromagnets $\text{ACo}_2\text{V}_2\text{O}_8$ ($A = \text{Ba}, \text{Sr}$), which have distorted CoO_6 octahedra, can be described in terms of a highly anisotropic effective $S = \frac{1}{2}$ 1D XXZ model in longitudinal fields^{5–9}. At high magnetic fields, a field-induced order-to-disorder transition above 1.8 K is observed. The quasi-2D ladder compound $\text{Na}_2\text{Co}_2(\text{C}_2\text{O}_4)_3(\text{H}_2\text{O})_2$ also contains distorted Co^{2+} octahedra. Its magnetic properties can be realized by a $S = \frac{1}{2}$ spin-ladder model and show spin-glass behavior^{10,11}.

Regarding spin-ladder structures, Co-based compounds are relatively rare compared to Fe- and Cu-based compounds. To our knowledge, besides $\text{Na}_2\text{Co}_2(\text{C}_2\text{O}_4)_3(\text{H}_2\text{O})_2$, the available examples are $\text{Co}(\text{C}_8\text{H}_8\text{O}_4)$, $\text{Co}_3(2,5\text{-pydc})_2(\mu_3\text{-OH})_2(\text{OH}_2)_2$ (*pydc* = pyridinedicarboxylate), $\text{Co}_7\text{V}_4\text{O}_{16}(\text{OH})_2(\text{H}_2\text{O})$ and $\text{Na}_{2-x}\text{Co}_6(\text{OH})_3[\text{HPO}_4][\text{H}_{x/3}\text{PO}_4]_3$ ^{11–13}. The properties of $\text{Co}(\text{C}_8\text{H}_8\text{O}_4)$ have not been measured, while the rest of them exhibit an antiferromagnetic ordering far below room temperature. Apart from 2-leg ladders, $\text{Co}(\text{H}_2\text{O})\{\text{C}_5\text{H}_5\text{N-CH}_2\text{CH}(\text{OH})(\text{PO}_3)(\text{PO}_3\text{H})\}$ contains zigzag ladders (see the schematic drawing in Fig. 1a), having frustration within the ladders¹⁴. According to magnetic susceptibility measurements, it shows no magnetic ordering down to 1.8 K, while a field-induced phase transition is observed at about 1.5 T. Necklace ladders (see Fig. 1b), which can be regarded as 3-leg zigzag ladders, are so far not found in Co-based compounds but in some Cu-based materials like ferrimagnets $\text{A}_3\text{Cu}_3(\text{PO}_4)_4$ ($A = \text{Ca}, \text{Sr}, \text{Pb}$)¹⁵.

In this report, the novel ladder-type compound $\text{Sr}_2\text{Co}_3\text{S}_2\text{O}_3$ is investigated. It demonstrates a new orthorhombic crystal structure type. In Co–O layers, the unique combination of 2-leg rectangular ladders and necklace ladders constructs a *hybrid spin ladder*, a new type of spin ladder. Further, a rare local symmetry of Co^{2+} , meridional heteroleptic octahedral coordination by three O^{2-} and three S^{2-} ions, is revealed. With the measurements of magnetic properties and specific heat, an antiferromagnetic transition is found close to room temperature

Max Planck Institute for Chemical Physics of Solids, Nöthnitzer Str. 40, 01187 Dresden, Germany. Correspondence and requests for materials should be addressed to K.T.L. (email: kt.lai@cpfs.mpg.de)

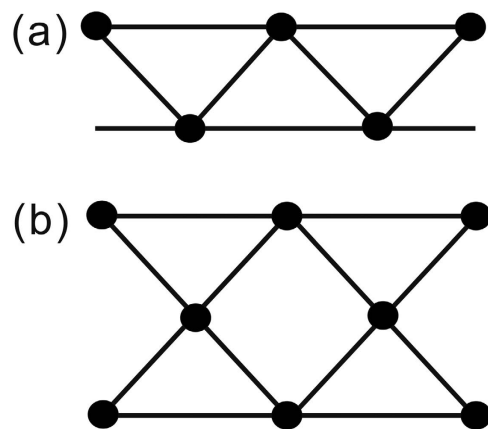


Figure 1. The schematic drawings of (a) a zigzag lattice and (b) a necklace ladder. The dots represent magnetic ions.

($T_N \sim 267$ K) along with a broad maximum in magnetic susceptibility below T_N . The broad maximum hints at the possible coexistence of spin ordering and short-range ordering below T_N , where the short-range ordering may be formed from dimers with an effective $S = \frac{1}{2}$.

Results

Crystal structure. Based on single crystal and powder x-ray diffraction, $\text{Sr}_2\text{Co}_3\text{S}_2\text{O}_3$ is determined as a new-type orthorhombic structure with a space group of $Pbam$, which is illustrated in Fig. 2a. The single crystal refinement details are presented in Table 1, while the corresponding atomic parameters can be found in Tables 2 and 3. The powder x-ray diffraction data and simulated Rietveld pattern are shown in Fig. 3. The Bragg peaks according to the crystal structure model obtained from the single crystal x-ray diffraction can be well assigned in the powder x-ray diffraction pattern except the peaks from a small amount of CoO impurity ($\sim 1\%$). This is suggestive of a high-quality powder sample. Note that the broad low-angle scattering comes from the sample holder. The elemental analysis from the energy-dispersive x-ray spectroscopy (see Supplementary information) also supports that the sample's composition is consistent with the nominal composition.

The different aspects of the crystal structure of $\text{Sr}_2\text{Co}_3\text{S}_2\text{O}_3$ are illustrated in Fig. 2. Due to anion ordering of O and S, a classical structural description starting from a close packing is inappropriate. In a local description, Co^{2+} is exclusively octahedrally coordinated, either by *mer*- $[\text{CoS}_{3/5}\text{O}_{2/3}\text{O}_{1/2}]^{2+}$ in Co2 sites (Fig. 2b) or by *trans*- $[\text{CoS}_{4/5}\text{O}_{2/3}]^{2+}$ in Co1 sites (Fig. 2c). The former (Co2) constitutes the 2-leg ladder while the latter (Co1) contributes the central spin chain in the necklace ladder (Fig. 2d). The 2-leg ladder and the necklace ladder share the common legs. This unique combination can be referred to as a *hybrid spin ladder*. The Co octahedra build up a three dimensional network by sharing faces and vertices. The interatomic distances are on average: Co–O = 2.0 Å and Co–S = 2.7 Å. These are different from comparable distances in ionic compounds like NaCl-type CoO (Co–O = 2.13 Å)¹⁶ and NiAs-type CoS (Co–S = 2.34 Å)¹⁷. The relatively short Co–O and long Co–S distances indicate anomalous bonding behavior, which is accompanied with low local symmetry at the *mer*-coordinated Co site. The shortest Co–Co distance, across face-sharing octahedra, is about 2.9 Å, which is too long for any direct magnetic interactions. Nine-fold coordinated Sr^{2+} ions act as space fillers.

The Co–O–Co angles within the 2-leg ladder are $\angle 180^\circ$ for the rungs and $\sim 169^\circ$ for the legs, forming almost ideal rectangular ladders. Meanwhile, the Co–O–Co angles within the necklace ladders are $\sim 94^\circ$. Between the 2-leg ladders there is no geometrical frustration, i.e. the rungs have the same periodicity in the *ac*-plane, but the *hybrid spin ladder* is frustrated due to intrinsic frustration within the necklace ladders. Three layers of the *hybrid spin ladders*, as displayed in Fig. 4a, reveal the connection perpendicular to the serrated *hybrid* layers. The inter-layer couplings are possible via Co–S–Co with $\sim 130^\circ$.

Before leaving this section, we would like to remark that the oxidation state and spin state of Co ions in $\text{Sr}_2\text{Co}_3\text{S}_2\text{O}_3$ are expected to be +2 (d^7) and high spin ($S = \frac{3}{2}$) in virtue to the charge balance deduced from the composition and the relatively large Co-octahedra.

Magnetic properties and specific heat of polycrystals. Figure 5 shows the temperature dependence of magnetic susceptibility $\chi(T)$ and specific heat $C_p(T)$ of polycrystalline $\text{Sr}_2\text{Co}_3\text{S}_2\text{O}_3$, respectively. It is obvious in the result from $C_p(T)$ (Fig. 5b) that there is a λ -type peak at $T \sim 267$ K (denoted as T_N). Due to the absence of hysteresis comparing the measurements between increasing and decreasing temperature as shown in the inset of Fig. 5b, T_N indicates a second order phase transition. T_N can be also visible in $\chi(T)$ (Fig. 5a) that a small hump is observed around T_N . A clearer picture can be seen in the plot of the first derivative of magnetic susceptibility $\chi'(T)$ in the inset in Fig. 5a, which indicates a significant change in $\chi(T)$ at T_N . These data suggest that T_N corresponds to a magnetic phase transition. The magnetic entropy released from T_N , ΔS_{mag} , is calculated to be about $2.26 \text{ J mol}^{-1} \text{ K}^{-1}$ by using the integral $\Delta S_{mag} = \int C_{mag}/T dT$, where the magnetic contribution of specific heat C_{mag} is obtained by subtracting the phononic background in the total specific heat. Since there is lack of non-magnetic

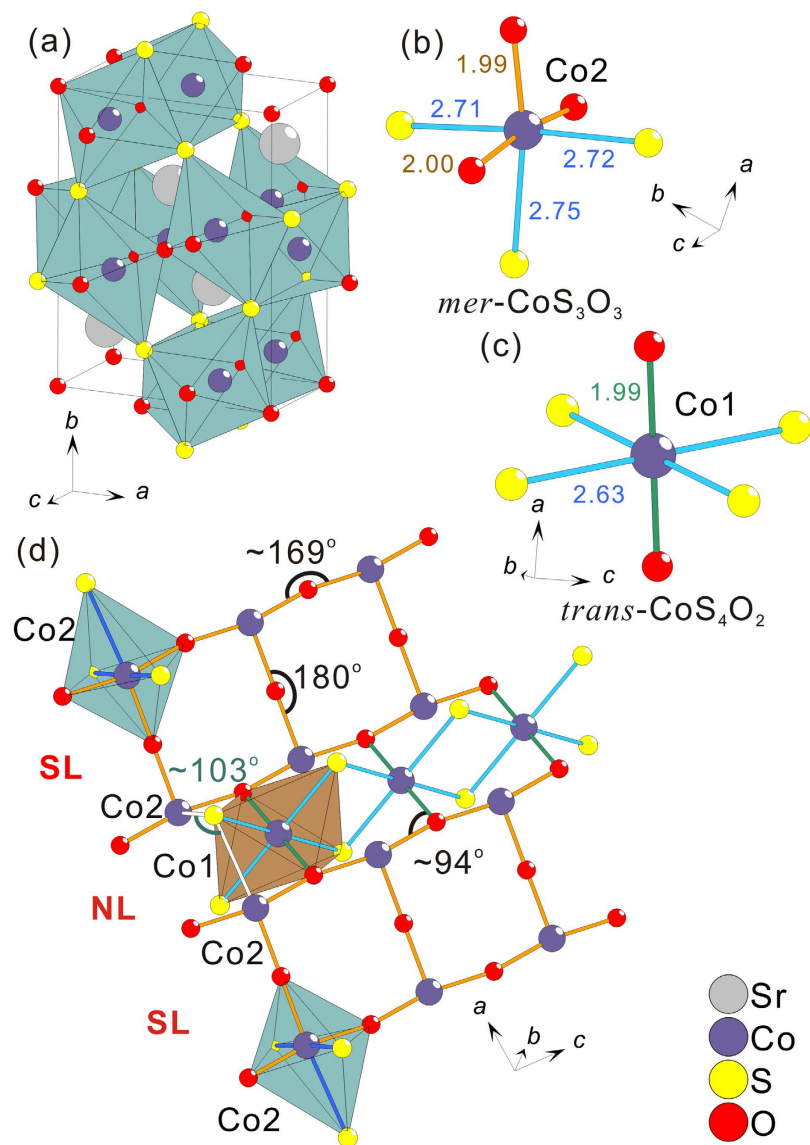


Figure 2. The schematic drawings of crystal structure of $\text{Sr}_2\text{Co}_3\text{S}_2\text{O}_3$. (a) The unit cell. (b) The *mer*- CoS_3O_3 octahedral coordination in the Co2 site. (c) The *trans*- CoS_4O_2 octahedral coordination in the Co1 site. The interatomic distances are in Å. (d) The Co-O hybrid spin ladder composed of rectangular two-leg ladders (SL) and necklace ladders (NL) alternatively along *ac*-plane.

isostructural compounds as a reference for the phononic contribution, the background is roughly defined by the specific heat below the dashed line shown in the inset in Fig. 5b. The obtained value is much smaller than the theoretical value $R \ln(2S+1) \sim 11.5 \text{ J mol}^{-1} \text{ K}^{-1}$, where $R = 8.31 \text{ J mol}^{-1} \text{ K}^{-1}$ is the gas constant. However, considering the purity of the sample, it is safe to assume that this magnetic entropy belongs to the title compound. The small magnetic entropy is typical for low-dimensional systems that ΔS_{mag} is released in a wide temperature range around the peak. In addition to the rough approximation in our analysis, the phonon contribution is hence easily overestimated and results in the small value of ΔS_{mag} . Therefore, it is not possible to determine from ΔS_{mag} whether all the Co spins order at T_N .

At $T < T_N$, $\chi(T)$ demonstrates a broad maximum around 70 K and approaches to the lowest value but non-zero around 2 K. Meanwhile, there are no anomalies in $C_p(T)$ ranged from $2 \text{ K} \leq T < T_N$, disproving the presence of any further obvious phase transitions below T_N . At $T > T_N$, $C_p(T)$ saturates at $3NR \sim 250 \text{ J mol}^{-1} \text{ K}^{-1}$ (except the entropy release from the transition), which agrees with the Dulong-Petit limit. Here $N = 10$ is the number of independent atoms in the unit cell. The inverse magnetic susceptibility $\chi^{-1}(T)$ at the range $T_N < T < 750 \text{ K}$, as illustrated in Fig. 6, is not linear, which can be explained by the fact that the first excited orbital levels are thermally populated in this temperature range¹⁸.

We would like to remark that $\text{Sr}_2\text{Co}_3\text{S}_2\text{O}_3$ is highly insulating ($>5 \text{ k}\Omega\text{m}$) at room temperature, which is expected for a high-spin Co^{2+} oxide.

Empirical formula	Sr ₂ Co ₃ S ₂ O ₃
Crystal system	Orthorhombic
Space group	<i>Pbam</i> (No. 55)
<i>Z</i>	2
<i>a</i> (Å)	7.50285(4)
<i>b</i> (Å)	9.79549(5)
<i>c</i> (Å)	3.99006(2)
<i>V</i> (Å ³)	293.246(3)
Calculated density (g/cm ³)	5.2567
Range of data collection	3.42 ≤ 2θ ≤ 65.84
No. of measured reflections	2785
No. of independent reflections	1552
No. of refined parameters	33
<i>h, k, l</i> ranges	0 ≤ <i>h</i> ≤ 19, 0 ≤ <i>k</i> ≤ 25, 0 ≤ <i>l</i> ≤ 10
μ (mm ⁻¹)	27.024
<i>R</i> (obs), <i>R_w</i> (obs)	0.033, 0.090
<i>R</i> (all), <i>R_w</i> (all)	0.050, 0.14
Goodness of fit	0.70
Final difference density	+0.90/−2.78
Data base - CSD number ^d	431714

Table 1. Details on the single crystal refinement of Sr₂Co₃S₂O₃ at room temperature. ^aFurther details of the crystal structure investigations may be obtained from FIZ Karlsruhe, 76344 Eggenstein-Leopoldshafen, Germany (fax: (+49)7247-808-666; e-mail: crysdata@fiz-karlsruhe.de, on quoting the CSD numbers).

Atom	Wyckoff	<i>x</i>	<i>y</i>	<i>z</i>	<i>U_{eq}</i>
Sr1	4 <i>h</i>	0.09375(4)	0.15762(3)	0.5	0.00617(4)
Co1	2 <i>d</i>	0	0.5	0.5	0.00822(9)
Co2	4 <i>g</i>	0.25962(5)	0.41255(4)	0	0.00716(6)
S1	4 <i>g</i>	0.4051(1)	0.15825(7)	0	0.0066(1)
O1	2 <i>a</i>	0	0	0	0.0074(5)
O2	4 <i>h</i>	0.2341(3)	0.4085(2)	0.5	0.0069(3)

Table 2. Atomic positions of Sr₂Co₃S₂O₃.

Atom	<i>U₁₁</i>	<i>U₂₂</i>	<i>U₃₃</i>	<i>U₁₂</i>	<i>U₁₃</i>	<i>U₂₃</i>
Sr1	0.00657(8)	0.00687(8)	0.00507(8)	−0.00011(6)	0	0
Co1	0.0055(1)	0.0100(2)	0.0092(2)	0.0022(1)	0	0
Co2	0.0069(1)	0.0110(1)	0.00356(9)	−0.00216(9)	0	0
S1	0.0068(2)	0.0075(2)	0.0056(2)	−0.0003(2)	0	0
O1	0.0054(7)	0.0102(9)	0.0067(8)	0.0011(7)	0	0
O2	0.0068(5)	0.0098(6)	0.0042(5)	0.0002(5)	0	0

Table 3. Anisotropic displacement parameters of Sr₂Co₃S₂O₃.

Discussion

The uniqueness of the crystal structure of Sr₂Co₃S₂O₃ are twofold: the meridional (*mer*) heteroleptical octahedral coordination in a magnetic ion and the *hybrid spin ladder*. *Mer*-octahedral coordinations can be found in some metal organic complexes, with either homoleptic coordination by N in e.g. *mer*-[Co(dien)(NO₂)₃] (dien = diethylenetriamine)¹⁹, [Co(dien)₂]X₃ · 2H₂O (*X* = Cl, Br)²⁰ and *mer*-[Ni(dien)₂][SCN]₂²¹ or heteroleptic coordination by N and O in [Cr(HP₂O₇)(NH₃)₃(H₂O)] · 2H₂O²². For non-complex inorganic materials, the *mer*-heteroleptic coordination exists in M₂[Nb₃O₅X₇] (*M* = NH₄, K, Rb, Cs; *X* = Cl, Br) and in La₆Ti₃S₈O₅, where the octahedra are composed by a Nb⁵⁺ (Ti⁴⁺) ion surrounding by three O²⁻ and three X^(S²⁻) ions^{23–25}. According to powder x-ray diffraction data and theoretical calculations, *mer*-Ta₂N₃O₃ octahedra are also reported in diamagnetic γ- and δ-TaON^{26,27}. However, due to the *d*⁰ configuration of the Nb⁵⁺, Ta⁵⁺ and Ti⁴⁺ ions, those compounds should be diamagnetic. Hence, Sr₂Co₃S₂O₃ is, to our knowledge, the first case where a magnetic ion, here high-spin Co²⁺, is heteroleptically *mer*-octahedrally coordinated in an extended lattice. *Mer*-coordination for *d*⁰, *d*⁵ or *d*¹⁰ systems is within expectations due to spherical symmetry of these ions. However, it is exceptional to discover such

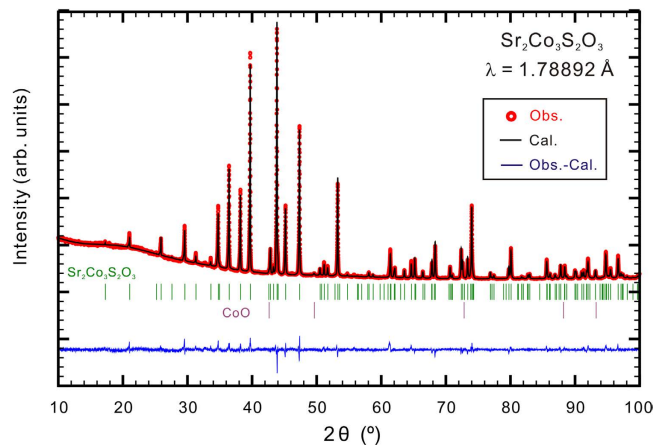


Figure 3. The powder x-ray diffraction pattern of $\text{Sr}_2\text{Co}_3\text{S}_2\text{O}_3$ at room temperature.

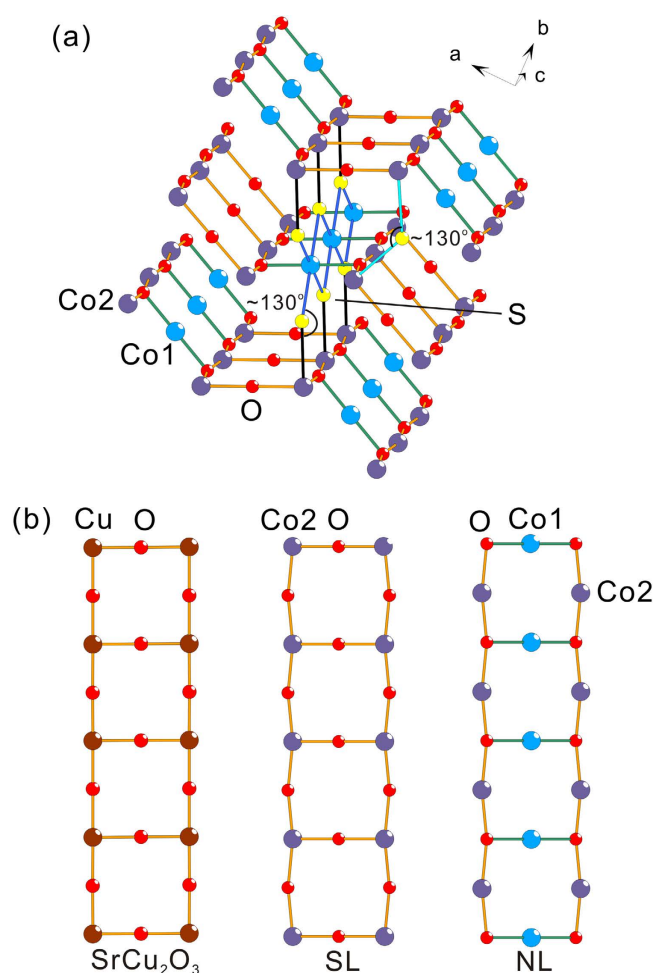


Figure 4. (a) The crystal structure of $\text{Sr}_2\text{Co}_3\text{S}_2\text{O}_3$ with 3 layers of the Co-O hybrid spin ladders. The interlayer bondings with darker color represent the Co1-Co2 interlayer coupling, while that with light color represent the Co2-Co2 interlayer coupling. (b) The comparison of ladder lattices among (left) the spin ladder in SrCu_2O_3 ²⁹, (middle) the 2-leg rectangular ladder in $\text{Sr}_2\text{Co}_3\text{S}_2\text{O}_3$ and (right) the necklace ladder in $\text{Sr}_2\text{Co}_3\text{S}_2\text{O}_3$.

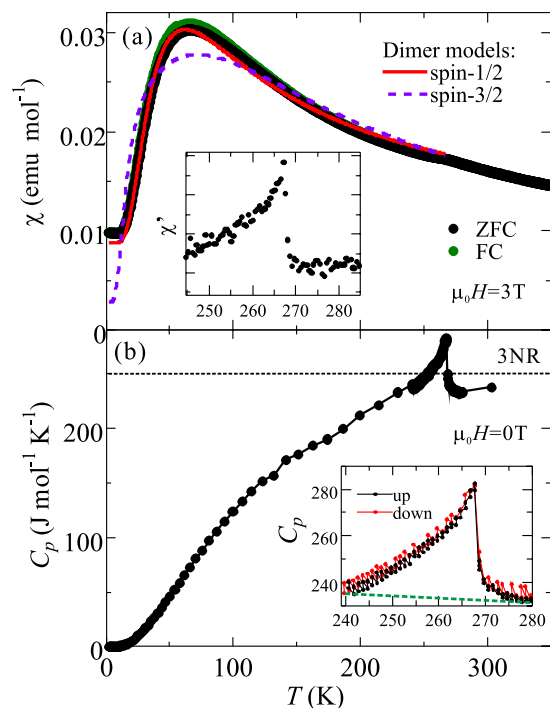


Figure 5. (a) The temperature dependence of magnetic susceptibility $\chi(T)$ of polycrystalline $\text{Sr}_2\text{Co}_3\text{S}_2\text{O}_3$ at 3 T. The dots represent the observed data, while the solid line and the dashed line are the fitted curves according to the $S = \frac{1}{2}$ dimer model (Eq. 2) and the $S = \frac{3}{2}$ dimer model (Eq. 3), respectively. The inset shows the first derivative of magnetic susceptibility $\chi'(T)$ under zero field cooling. (b) The temperature dependence of specific heat $C_p(T)$ of polycrystalline $\text{Sr}_2\text{Co}_3\text{S}_2\text{O}_3$ at zero field. The dotted line indicates the Dulong-Petit limit. The inset displays the comparison of the measurements of $C_p(T)$ with increasing and decreasing temperatures around the transition. The dashed line is an estimate of the phononic contribution.

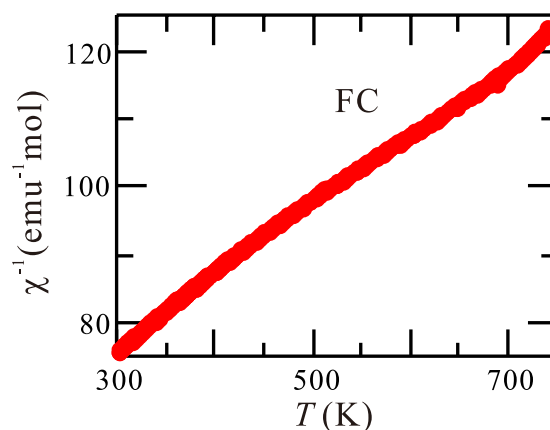


Figure 6. The temperature dependence of inverse magnetic susceptibility $\chi^{-1}(T)$ at $T > 300$ K under field cooling.

coordination for a d^7 system, because of the uneven electronic occupancy of the d -orbitals. Hence, the situation in $\text{Sr}_2\text{Co}_3\text{S}_2\text{O}_3$ offers the possibility to investigate the effect of a rare crystal field on a magnetic ion.

The *hybrid spin ladder* is the combination of a 2-leg ladder and a necklace ladder. The former is reminiscent of those in cuprates like La_2CuO_4 , SrCu_2O_3 and $\text{Sr}_2\text{Cu}_3\text{O}_5$ ^{28,29} (Fig. 4b). The necklace ladder can be regarded as the inverse version of the 2-leg ladder (Fig. 4b) and is related to the Cu lattice in $\text{A}_3\text{Cu}_3(\text{PO}_4)_4$ ($A = \text{Ca}, \text{Sr}, \text{Pb}$)¹⁵. However, the combination of the 2-leg ladders and the necklace ladders by sharing legs constructs a *hybrid spin ladder*, which is, to our knowledge, a new type of N -leg spin ladders. Its uniqueness in competing exchange interactions, including frustration, between magnetic ions can initiate further investigations of novel behaviors through the reproduction of the *hybrid spin ladder*.

In $\text{Sr}_2\text{Co}_3\text{S}_2\text{O}_3$, T_N is at relatively high temperature compared to other Co-based ladder compounds. This origin can be realized in the *mer*-coordination of the Co2 sites in the 2-leg ladders. Regarding the 2-leg ladders,

there are three crucial superexchange interactions: J_{rung} and J_{leg} connect Co^{2+} ions via Co–O–Co with about $\angle 180^\circ$ along the rungs and the legs in the 2-leg ladders, respectively (see Fig. 2d). J_{inter} transforms the quasi 1D 2-leg ladders into a 3D network via long Co–S–Co with $\angle 103\text{--}130^\circ$ (see Figs 2d and 4a). According to the Kanamori-Goodenough rules^{30,31}, J_{rung} and J_{leg} are expected to be antiferromagnetic interactions while J_{inter} can be antiferromagnetic or ferromagnetic but relatively weak. In addition to the frustration brought from the neighbor necklace ladders, the 2-leg ladders should be able to order antiferromagnetically but not at very high temperatures due to quantum fluctuations. However, as shown in Fig. 2b, the *mer*- CoS_3O_3 octahedron has low symmetry with respect to the Co ion. This gives a strongly anisotropic crystal field to the Co ion and thus a preferred orientation for the Co spin, which is referred to the phenomenon called single ion anisotropy. Therefore, although the 2-leg ladders are expected to suppress 3D magnetic orderings because of their low dimensionality, the easy axis for the Co spins in the *mer*-coordination is strong enough to favor the magnetic ordering at higher temperatures.

After the discussion of the spin ordering in the Co2 sites, it naturally comes to the question about the spin ordering of the remaining Co1 sites within the necklace ladders. The observation of the broad maximum in $\chi(T)$ below T_N provides a hint at a rare situation. If all the Co sites order at T_N , the broad maximum can stem from the spin canting at the two Co sites. However, this is unlikely due to the following reasons: First, the centrosymmetric space group does not allow for the residual ferromagnetic spin component by spin canting to result in the broad maximum. Second, the Co1 sites are geometrically frustrated. They should be less likely to order at such high T_N unless the spin ordering is somewhat much more energetically favorable. Furthermore, the Co1 sites have *trans*-octahedral coordination with compressed Jahn-Teller distortion (see Fig. 2c). In a rough approximation, the different crystal fields between the two Co sites suggest that they should have different ordering temperatures. This disagrees with the absence of further phase transitions below T_N as seen in $C_p(T)$. Alternatively, we propose that the Co1 sites could have no long-range ordering down to 2 K. In this framework, the broad maximum corresponds to short-range antiferromagnetic correlations for low-dimensional materials. Owing to the mirror plane on the *c*-axis for the centrosymmetric *Pbam* space group, spin dimer formation along the *c*-axis is a possible candidate for the short-range ordering on the Co1 sites.

To prove this argument, the data of $\chi(T)$ below T_N is fitted using the following relation:

$$\chi(T) = \chi_0 + \chi_{dimer} + \chi_{AFM}, \quad (1)$$

where, the first term χ_0 corresponds to temperature-independent Van-Vleck paramagnetism, diamagnetism and impurity contributions. The second term χ_{dimer} is the magnetic susceptibility arising from dimers at all the Co1 sites, which correspond to one magnetic Co^{2+} ion per formula. It is modelled by the following equations³²:

$$\chi_{dimer, S=\frac{1}{2}} = \frac{N_A g^2 \mu_B^2}{k_B T} \frac{2e^{2x}}{1 + 3e^{2x}} \quad (2)$$

for $S = \frac{1}{2}$ and

$$\chi_{dimer, S=\frac{3}{2}} = \frac{N_A g^2 \mu_B^2}{k_B T} \frac{2e^{2x} + 10e^{6x} + 28e^{12x}}{1 + 3e^{2x} + 5e^{6x} + 7e^{12x}} \quad (3)$$

for $S = \frac{3}{2}$, where N_A is Avogadro constant, μ_B is Bohr magneton, k_B is Boltzmann constant, g is the Landé *g*-factor and $x = J/k_B T$ with J being the nearest-neighbor intradimer exchange constant. The third term χ_{AFM} represents the magnetic susceptibility contributed from the antiferromagnetic ordering at all the Co2 sites, which correspond to two magnetic Co^{2+} ions per formula. Its temperature dependence is originally presumed according to the mean-field theory that χ_{AFM} gradually decreases with temperature and reaches $\frac{2}{3}$ of the value of $\chi_{AFM}(T = T_N)$ at $T = 0$ K for powder samples. However, it was found during the analysis that the temperature dependence of χ_{AFM} is much weaker than that of χ_{dimer} , leading to the difficulty of handling multiple free parameters. Hence, to reduce the number of free parameters, this term is thus regarded as temperature independent and refined together with χ_0 . Note that the Curie-Weiss contribution arising from the breakdown of dimers due to crystal defects is ignored since no upturn is observed at low temperatures (< 10 K).

The fitted curves for $S = \frac{1}{2}$ and $\frac{3}{2}$ are plotted in Fig. 5a. The curve for $S = \frac{3}{2}$ fails to fit the observed curve, rejecting the possibility for $S = \frac{3}{2}$ dimers. In contrast, the curve for $S = \frac{1}{2}$ agrees well with the broad maximum of $\chi(T)$. This is suggestive of the existence of quasi-1D dimers with an effective $S = \frac{1}{2}$ for octahedrally coordinated Co^{2+} ions. The slight discrepancy between the observed and fitted curves may stem from the complex dynamics between the antiferromagnetic ordering and the dimers as well as the oversimplified temperature dependence of χ_{AFM} . The parameters of the fitted curve for $S = \frac{1}{2}$ dimers are obtained as $g = 3.768(8)$, $J/k_B = -49.7(1)$ K and $\chi_0 + \chi_{AFM} = 0.00878(6)$ emu mol⁻¹. $g \gg 2$ supports the anisotropic feature of the effective $S = \frac{1}{2}$ in dimers. The relatively large J/k_B suggests that the antiferromagnetic interactions between dimers are strong. The value of $\chi_0 + \chi_{AFM}$ is close to the expected value (~ 0.008) of the magnetic susceptibility for the antiferromagnetically ordered Co sites (i.e. Co2 sites) at 0 K, agreeing with the assumption made in the fitting analysis.

In order to find out the experimental evidences for the existence of dimers, we have attempted to measure $\text{Sr}_2\text{Co}_3\text{S}_2\text{O}_3$ by nuclear magnetic resonance (NMR) and electron spin resonance (ESR) techniques. Unfortunately, there is no resolvable signal for further analysis, because the lifetime of nuclear and electronic spin excited states are too short and thus broaden the signal. Note that the existence of spin chains is excluded since no reasonable fits are obtained by using neither the model by Bonner and Fisher³³ nor the model from Padé approximations by Law *et al.*³⁴.

In conclusion, single crystalline and polycrystalline samples of $\text{Sr}_2\text{Co}_3\text{S}_2\text{O}_3$ were successfully synthesized. The compound is identified as a new-type structure with two interesting features. One is the unique *hybrid spin ladder* consisted of 2-leg ladders and necklace ladders. The other is the rare *mer*-heteroleptical octahedral coordination in magnetic Co^{2+} ions, providing a novel crystal field. Through magnetic property and specific heat measurements of the polycrystalline samples, an antiferromagnetic order forms at $T_N \sim 267$ K. Such high temperature for T_N is correlated to the highly anisotropic *mer*-coordination of the $\text{Co}2$ sites in the 2-leg ladders, which gives an easy axis for the Co spins to order at higher temperatures than other Co-based spin ladders. Below T_N , a broad maximum in $\chi(T)$ is observed along with the absence of further phase transitions. It is suggestive of the short-range magnetic correlations of the Co1 sites within the necklace ladders. The data analysis for the broad maximum proposes the possible coexistence of spin ordering and spin dimers with an effective $S = \frac{1}{2}$ below T_N . However, this has to be further confirmed by additional experimental investigations.

Methods

Synthesis. Polycrystalline $\text{Sr}_2\text{Co}_3\text{S}_2\text{O}_3$ was synthesized by solid state reaction using SrO, Co (Alfa Aesar 99.8%), Co_3O_4 (Alfa Aesar 99.7%) and S (Alfa Aesar 99.95%) as starting materials. SrO was obtained by heating SrCO_3 (Aldrich 99.9+%) at 1080 °C overnight at dynamic vacuum ($<10^{-4}$ mbar). The starting materials were mixed to homogeneity inside a dry argon filled glovebox ($\text{O}_2, \text{H}_2\text{O} < 1$ ppm). The mixture was then pressed into pellets and inserted into an alumina crucible. The crucible was inserted into a silica tube which was immediately evacuated to high vacuum ($\sim 10^{-4}$ mbar) and sealed. The sample was annealed at 1050 °C for 20 h. The reaction process was repeated 3 times with intermediate grinding but the annealing time was set to 10 h. Small plate-like single crystals were able to obtain by the similar procedures but were annealed at 1300 °C for 12 h following with cooling to 1050 °C in 96 h. The samples are black and stable in air.

Sample characterization. Single crystal x-ray diffraction of $\text{Sr}_2\text{Co}_3\text{S}_2\text{O}_3$ was performed in a Bruker Apex D8 Venture with a Mo- $K\alpha$ ($\lambda = 0.71073$ Å) radiation at room temperature. The numerical absorption correction was completed by using XRED (v. 1.07, STOE & Cie GmbH) and X-shape (v. 1.01, STOE & Cie GmbH). The crystal structure was determined and refined by treating the single crystal x-ray diffraction data with the JANA2006 software³⁵. The powder x-ray diffraction was carried out in a focusing camera with a Co ($\lambda = 1.78892$ Å) radiation. The corresponding Rietveld refinement was also performed in JANA2006. Elemental analysis was conducted in an energy-dispersive x-ray spectroscopy (EDX) inside a scanning electron microscope (Philips SEM XL30).

Measurements of physical properties. The magnetic properties of the polycrystalline samples were measured by a magnetic property measurement system (Quantum Design MPMS XL). For $T > 350$ K, a furnace was inserted for additional heating. The specific heat measurements were performed in a physical property measurement system (Quantum Design PPMS) with the standard non-adiabatic thermal relaxation technique.

References

1. Abragam, A. & Bleaney, B. *Electron Paramagnetic Resonance of Transition Ions* (Clarendon, 1970).
2. Abragam, A. & Pryce, M. H. L. The theory of paramagnetic resonance in hydrated cobalt salts. *Proc. Roy. Soc.* **A206**, 173–191 (1951).
3. Lines, M. E. Magnetic properties of CoCl_2 and NiCl_2 . *Phys. Rev.* **131**, 546 (1963).
4. Carlin, R. L. *Magnetochemistry* (Springer, 1986).
5. He, Z., Taniyama, T., Kyomen, T. & Itoh, M. Field-induced order-disorder transition in the quasi-one-dimensional anisotropic antiferromagnet $\text{BaCo}_2\text{V}_2\text{O}_8$. *Phys. Rev. B* **72**, 172403 (2005).
6. Kimura, S. *et al.* Field-induced order-disorder transition in antiferromagnetic $\text{BaCo}_2\text{V}_2\text{O}_8$ driven by a softening of spinon excitation. *Phys. Rev. Lett.* **99**, 087602 (2007).
7. He, Z., Taniyama, T., Kyomen, T. & Itoh, M. Antiferromagnetic-paramagnetic transitions in longitudinal and transverse magnetic fields in a $\text{SrCo}_2\text{V}_2\text{O}_8$ crystal. *Phys. Rev. B* **73**, 212406 (2006).
8. Bera, A. K., Lake, B., Stein, W.-D. & Zander, S. Magnetic correlations of the quasi-one-dimensional half-integer spin-chain antiferromagnets $\text{SrM}_2\text{V}_2\text{O}_8$ ($M = \text{Co}, \text{Mn}$). *Phys. Rev. B* **89**, 094402 (2014).
9. Wang, Z. *et al.* Spinon confinement in the one-dimensional Ising-like antiferromagnet $\text{SrCo}_2\text{V}_2\text{O}_8$. *Phys. Rev. B* **91**, 140101(R) (2015).
10. Honda, Z., Katsumata K., Kikkawa A. & Yamada, K. Thermodynamic properties in the approach to the quantum critical point of the spin-ladder material $\text{Na}_2\text{Co}_2(\text{C}_2\text{O}_4)_3(\text{H}_2\text{O})_2$. *Phys. Rev. Lett.* **95**, 087204 (2005).
11. Kurmoo, M. Magnetic metal-organic frameworks. *Chem. Soc. Rev.* **38** 1353–1379 (2009).
12. Zhang, S.-Y. *et al.* Synthesis, crystal structure and magnetic property of a new cobalt(II)vanadate. *J. Solid State Chem.* **225**, 78–82 (2015).
13. Yakubovich, O. V. *et al.* A novel cobalt sodium phosphate hydroxide with the ellenbergerite topology: crystal structure and physical properties. *Dalton Trans.* **44**, 11827 (2015).
14. Zhang, Z.-C., Gao, S. & Zheng, L.-M. Cobalt diphosphonate with a new double chain structure exhibiting field-induced magnetic transition. *Dalton Trans.* 4681–4684 (2007).
15. Yamamoto, S. & Ohara, J. Low-energy structure of the homometallic intertwining double-chain ferrimagnets $\text{A}_3\text{Cu}_3(\text{PO}_4)_4$ ($A = \text{Ca}, \text{Sr}, \text{Pb}$) *Phys. Rev. B* **76**, 014409 (2007).
16. Jauch, W., Reehuis, M., Bleif, H. J., Kubanek, F. & Pattison, P. Crystallographic symmetry and magnetic structure of CoO . *Phys. Rev. B* **64**, 052102 (2001).
17. Lundqvist, D. & Westgren, A. Roentgenuntersuchung des Systems Co-S. *Z. Anorg. Allg. Chem.* **239**, 85–85 (1938).
18. Burnus, T. *et al.* Local electronic structure and magnetic properties of $\text{LaMn}_{0.5}\text{Co}_{0.5}\text{O}_3$ studied by x-ray absorption and magnetic circular dichroism spectroscopy. *Phys. Rev. B* **77**, 125124 (2008).
19. Churchill, M. R., Harris, G. M., Inoue, T. & Lashewycz, A. The meridional isomer of (diethylenetriamine)trinitrocobalt(III), *mer*-[Co(dien)(NO₂)₃]. *Acta Crystallogr.* **B37**, 933–934 (1981).
20. Keene, F. R. & Searle, G. H. The isomers of the Bis(diethylenetriamine)cobalt(III) ion and a new source of optical activity. *Inorg. Chem.* **11**, 148–156 (1972).
21. Mukherjee, A. K. *et al.* Isomerism in Bis(diethylenetriamine)nickel(II) thiocyanate: synthesis, solid-state interconversion and x-ray crystallographic study of *sym-fac* and *mer* isomers. *J. Chem. Soc., Dalton Trans.* **16**, 2367–2371 (1994).

22. Haromy, T. P., Linck, C. F., Cleland, W. W. & Sundaralingam, M. Structures of the meridional and facial isomers of triamminechromium pyrophosphate dihydrate. *Acta Crystallogr.* **C46**, 951–957 (1990).
23. Reusch, U. & Schweda, E. Preparation and crystal structure of diammonium heptachloropentaoxotrinobate(V) $(\text{NH}_4)_2[\text{Nb}_3\text{O}_5\text{X}_7]$. *Z. Anorg. Allg. Chem.* **623**, 805–809 (1997).
24. Beck, J., Bordinhão, J. & Kusterer, C. On oxohalogeno niobates(V) $M_2[\text{Nb}_3\text{O}_5\text{X}_7]$ ($M = \text{NH}_4, \text{K}, \text{Rb}, \text{Cs}; \text{X} = \text{Cl}, \text{Br}$) - new members of a compound family with a layered structure. *Z. Anorg. Allg. Chem.* **633**, 757–762 (2007).
25. Cody, J. A. & Ibers, J. A. Synthesis and characterization of the new rare-earth/transition-metal oxysulfides $\text{La}_6\text{Ti}_2\text{S}_8\text{O}_5$ and $\text{La}_4\text{Ti}_3\text{S}_4\text{O}_8$. *J. Solid State Chem.* **114**, 406–412 (1995).
26. Schilling, H. *et al.* γ -TaON: A metastable polymorph of tantalum oxynitride. *Angew. Chem. Int. Ed.* **46**, 2931–2934 (2007).
27. Lüdtkke, T. *et al.* Synthesis and crystal structure of δ -TaON, a metastable polymorph of tantalum oxide nitride. *Inorg. Chem.* **53**, 11691–11698 (2014).
28. Longo, J. M. & Raccach, P. M. The structure of La_2CuO_4 and LaSrVO_4 . *J. Solid State Chem.* **6**, 526–531 (1973).
29. Dagotto, E. & Rice, T. M. Surprises on the way from one- to two-dimensional quantum magnets: the ladder materials. *Science* **271**, 618–623 (1996).
30. Kanamori, J. Superexchange interaction and symmetry properties of electron orbitals. *J. Phys. Chem. Solids* **10**, 87–98 (1959).
31. Goodenough, J. B. Theory of the role of covalence in the perovskite-type manganites $[\text{La}, \text{M}(\text{II})]\text{MnO}_3$. *Phys. Rev.* **100**, 564–573 (1955).
32. O'Connor, C. J. Magnetochemistry-advances in theory and experimentation. *Prog. Inorg. Chem.* **29**, 203–283 (1982).
33. Bonner, J. C. & Fisher, M. E. Linear magnetic chains with anisotropic coupling. *Phys. Rev.* **135**, A640 (1964).
34. Law, J. M., Benner, H. & Kremer, R. K. Padé approximations for the magnetic susceptibilities of Heisenberg antiferromagnetic spin chains for various spin values. *J. Phys.: Condens. Matter* **25**, 065601 (2013).
35. Petříček, V., Dušek, M. & Palatinus L. Crystallographic computing system JANA2006: general features. *Z. Kristallogr.* **229**(5), 345–352 (2014).

Acknowledgements

The authors thank Liu Hao Tjeng for fruitful discussions and Ulrich Burkhardt for the measurement of EDX analysis. We also thank Michael Baenitz and Hiroshi Yasuoka for the trials of NMR measurements, and Jörg Sichelshmidt for the trials of ESR measurements.

Author Contributions

K.T.L. and M.V. wrote the manuscript and conceived the experiments. K.T.L. conducted the synthesis, the measurements of powder x-ray diffraction, magnetic properties and specific heat. M.V. conducted the measurement of single crystal x-ray diffraction. K.T.L. and M.V. analysed the results of x-ray diffraction, magnetic properties and specific heat data. All authors reviewed the manuscript.

Additional Information

Supplementary information accompanies this paper at <http://www.nature.com/srep>

Competing Interests: The authors declare no competing financial interests.

How to cite this article: Lai, K. T. and Valldor, M. Coexistence of spin ordering on ladders and spin dimer formation in a new-structure-type compound $\text{Sr}_2\text{Co}_3\text{S}_2\text{O}_3$. *Sci. Rep.* **7**, 43767; doi: 10.1038/srep43767 (2017).

Publisher's note: Springer Nature remains neutral with regard to jurisdictional claims in published maps and institutional affiliations.



This work is licensed under a Creative Commons Attribution 4.0 International License. The images or other third party material in this article are included in the article's Creative Commons license, unless indicated otherwise in the credit line; if the material is not included under the Creative Commons license, users will need to obtain permission from the license holder to reproduce the material. To view a copy of this license, visit <http://creativecommons.org/licenses/by/4.0/>

© The Author(s) 2017